Regulation of Cohesin-Mediated Chromosome Folding by Eco1 and Other Partners

Lise Dauban, Rémi Montagne, Agnès Thierry, Luciana Lazar-Stefanita, Nathalie Bastié, Olivier Gadal, Axel Cournac, Romain Koszul, Frederic Beckouet

Regulation of cohesin-mediated chromosome folding by Eco1 and other partners

Lise Dauban[4,&], Rémi Montagne[1,2,&], Agnès Thierry[1,2,&], Luciana Lazar-Stefanita[1,2,3,#], Nathalie Bastié[4], Olivier Gadal[4], Axel Cournac[1,2], Romain Koszul[1,2,5*] and Frédéric Beckouët[4,*]

[1]Institut Pasteur, Unité Régulation Spatiale des Génomes, UMR 3525, CNRS, Paris, F-75015, France

[2]Institut Pasteur, Center of Bioinformatics, Biostatistics and Integrative Biology (C3BI), Paris, F-75015, France

[3]Sorbonne Université, Collège Doctoral, F-75005 Paris, France

[4]Laboratoire de Biologie Moléculaire Eucaryote, Centre de Biologie Intégrative (CBI), Université de Toulouse, CNRS, UPS, 31000, Toulouse, France

[5]Lead contact

*Corresponding authors: romain.koszul@pasteur.fr and frederic.beckouet@ibcg.biotoul.fr

[&]these authors contributed equally to this work

#present address: Institute for Systems Genetics and Department of Biochemistry and Molecular Pharmacology, NYU Langone Health, New York, NY 10016, USA

SUMMARY

Cohesin, a member of the SMC complex family, holds sister chromatids together but also shapes chromosomes by promoting the formation of long-range intra-chromatid loops, a process proposed to be mediated by DNA loop extrusion. Here we describe the roles of three cohesin partners Pds5, Wpl1 and Eco1 in loop formation along either unreplicated or mitotic *Saccharomyces cerevisiae* chromosomes. Pds5 limits the size of DNA loops *via* two different pathways: the canonical Wpl1-mediated releasing activity, and an Eco1-dependent mechanism. In the absence of Pds5, the main barrier to DNA loop expansion appears to be the centromere. Our data also show that Eco1 acetyl-transferase inhibits the translocase activity that powers loop formation and contributes to the positioning of loops, through a mechanism that is distinguishable from its role in cohesion establishment. This study reveals that the mechanisms regulating cohesin-dependent chromatin loops are conserved among eukaryotes, while promoting different functions.

INTRODUCTION

Recent advances in imaging and chromosome conformation capture techniques (3C, Hi-C; (Dekker et al., 2002)) have unveiled a hierarchy of chromatin structural arrangements (Cavalli and Misteli, 2013; Dekker and Mirny, 2016; Yu and Ren, 2017). A variety of megabase (Mb) and sub-Mb structures have been proposed to organize the chromosomes of bacteria (Le et al., 2013; Lioy et al., 2018; Marbouty et al., 2015), yeasts (Lazar-Stefanita et al., 2017; Mizuguchi et al., 2014; Muller et al., 2018; Schalbetter et al., 2017) and mammals (Dekker and Mirny, 2016; Yu and Ren, 2017) and are presumably a feature of most if not all organisms. During mitosis, this organization undergoes its most radical change when chromatin is transformed in condensed thread-like structures that facilitate chromosome segregation (Liang et al., 2015).

In many species, the cohesin and condensin SMC protein complexes play important roles in chromosome folding. They consist of a pair of SMC proteins that associate with a Kleisin protein to form a large tripartite ring capable of embracing one or two DNA molecules (Nasmyth and Haering, 2009). In addition to mediating sister chromatid cohesion during G2/M phases of the cell cycle (Gligoris et al., 2014; Haering et al., 2008), cohesin shares with condensin the ability to convert DNA fibers into chromatid thread-like structures through a mechanism that remains poorly understood (Kagey et al., 2010; Parelho et al., 2008; Wutz et al., 2017). SMC rings may organize DNA within chromatids by a DNA loop extrusion process, which consists in capturing small chromatin loops and progressively catalyzing their enlargement into large, megabase-sized structures (Fudenberg et al., 2016; Gibcus et al., 2018; Nasmyth, 2001). The precise mechanisms driving the generation of loops remain however to be fully characterized.

In mammals, condensin-dependent loops represent basic units for the folding of mitotic chromosomes into compact, higher-order chromatin structures. Cohesin-dependent loops, on the other hand, appear to contribute to long-range gene regulation in interphase, and to the segmentation of interphase chromosomes into topologically associating domains (TADs) defined as sub-megabase self-interacting regions. The organization of interphasic chromosomes into self-interacting domains has been proposed to insulate enhancers from non-cognate promoters by blocking cohesin-dependent loop progression when cohesin reaches the insulator protein CTCF bound to DNA (Nora et al., 2017). Interphasic self-interacting domains are chromosomal features found in many studied living organisms but their dependency on cohesin and CTCF activities is not automatic. Besides mammals, the involvement of cohesin in domain formation has for instance been reported in fission yeast (Mizuguchi et al., 2014). In budding yeast *S. cerevisiae* however, no clear TADs-like structure nor DNA loops have been identified along interphase chromosomes. Nevertheless, the fact that cohesin is essential to convert the rDNA locus into a thread-like structure (Guacci et al., 1994) during mitosis raises the idea that cohesin may also mediate cis-DNA looping along the yeast chromosome. Recently, we and others showed using Hi-C that meiotic and mitotic compaction in budding yeast is dependent on cohesin (Lazar-Stefanita et al., 2017; Muller et al., 2018; Schalbetter et al., 2017). Surprisingly, we also found that condensin is dispensable for mitotic chromosome arm compaction. Instead, condensin is required for higher-order chromatin structuring at the rDNA locus during anaphase and for promoting resolution at peri-centromeric regions.

Cohesin is composed of two SMC ATPases (Smc1 and Smc3) and an α-kleisin subunit called Scc1/Rad21. This complex binds to DNA in a dynamic manner throughout the cell cycle. Cohesin loading requires ATP hydrolysis mediated by Scc2/NIPBL, that is thought to

result in entrapment of DNA inside the cohesin tripartite ring (Chapard et al., 2019; Ciosk et al., 2000; Gligoris et al., 2014; Haering et al., 2002; Hu et al., 2011). Cohesin may dissociate from DNA by separase-mediated cleavage of Scc1 at anaphase onset (Uhlmann et al., 1999) and in a manner that involves a "releasing activity" at other stages of the cell cycle. This separase-independent releasing activity relies on two cohesin-associated regulatory subunits: Wpl1/Wapl and Pds5 (Gandhi et al., 2006; Kueng et al., 2006; Rolef Ben-Shahar et al., 2008; Rowland et al., 2009). Pds5 binds within the N-terminal part of Scc1 and recruits Wpl1 (Chan et al., 2013) which opens the gate located between Scc1 and Smc3, triggering cohesin dissociation from DNA (Beckouët et al., 2016; Chan et al., 2012; Murayama and Uhlmann, 2015). When replication takes place, the releasing activity is repressed by Eco1-mediated acetylation of two conserved lysine residues (K112/113) within the Smc3 ATPase head (Rolef Ben-Shahar et al., 2008; Unal et al., 2008). This results in stabilization of cohesin on DNA and establishment of sister chromatid cohesion. It has been suggested that acetylation of K112/113 is in fact stimulated by both DNA replication fork progression and the Pds5 subunit (Beckouët et al., 2010; Chan et al., 2013; Rolef Ben-Shahar et al., 2008; Vaur et al., 2012). Smc3 acetylation is then maintained throughout G2 and M phases and only removed after cleavage of Scc1 and subsequent deacetylation by Hos1 (Beckouët et al., 2010).

If cohesin-mediated loops are established by loop extrusion, their lengths should depend on several parameters, notably cohesin residence time on DNA and an extrusion driving force. This prediction is supported by the observation that the length of chromatin loops in mammalian interphasic nuclei increases once cohesin turnover is abolished after inactivation of Wpl1 and Pds5 (Haarhuis and Rowland, 2017; Wutz et al., 2017). However, the mechanism(s) leading to loop enlargement remains a matter of debate. ATP hydrolysis may be the driving force for chromatin loop extrusion, as observed for the purified condensin

complex (Ganji et al., 2018). Scc2, being essential for cohesin's ATPase activity could thus play a key role in stimulating the translocation process and promoting DNA loop expansion (Petela et al., 2018). Alternatively, transcribing RNA polymerases may promote loop enlargement by pushing cohesin along the DNA (Busslinger et al., 2017; Lengronne et al., 2004). Finally, the frequency of cohesin injection along chromosomes may also influence their structure.

In the present study, we show that mitotic yeast chromosomes are compacted by cohesin dependent loops. By dissecting the roles of cohesin regulatory partners in DNA loop expansion, we also show that the mechanisms regulating loop positioning are highly conserved between yeast and mammals. Moreover, we find that in addition to promoting sister chromatid cohesion Eco1 inhibits the translocation process that extends DNA loops. In the absence of negative regulation, the main barrier to loop expansion is the centromere, which remains physically connected to the microtubule-organizing center (MTOC) during the entire yeast cell cycle.

RESULTS

Yeast mitotic chromosome arms are organized by cohesin-dependent loops

To characterize *S. cerevisae* mitotic chromosome organization we took advantage of yeast strains in which the cyclosome activator Cdc20 is under the control of the repressible MET3 promoter. To arrest the cells in mitosis, we released them from a G1 alpha-factor arrest by growing them in rich media supplemented with methionine (Figure 1A; Methods). Once arrested in metaphase, genome-wide chromatin contacts were quantified by Hi-C. Normalized contact maps (1 kb resolution) of mitotic chromosomes differed from G1 pattern in several ways (Figure 1B, left panels). First, the broad and thicker diagonal observed in metaphase

compared to G1 revealed increased contacts at short/medium range, blurring the boundaries of the small microdomains visible in G1. Second, discrete dots of variable intensities corresponding to enriched contacts between pairs of loci, consistent with DNA loops, were also often visible along mitotic chromosomes (Figure 1B, black arrows). Not all chromosomal regions were covered by a loop signal, but whether this results from the resolution of our experiment or a real feature of chromosome structure remains to be characterized. To better characterize chromosome compaction we computed the contact probability curve $P_c(s)$ for each condition (Lazar-Stefanita et al., 2017; Schalbetter et al., 2017) (Figure S1A; Methods). The derivative of the $P_c(s)$ curve in a log-log space can be used to facilitate the visualization of local differences (Methods). In mice, the maximum of the derivative curve also matches with the average length of extruded loops (Gassler et al., 2017). The same representation in yeast showed a net enrichment in mitosis in the contacts between loci separated by 30 kb or less, compared to G1 (Figure 1C, blue vs. orange curve). It also suggested a loop size in metaphase arrested cells of ~15 kb on average.

To directly test the role of cohesin in the maintenance of these structures, we depleted Scc1 in synchronized cells using an auxin degron strategy (Figure 1A right panel, Methods). Efficient Scc1 depletion was quantified by a split-dots assay measuring cohesion loss (Figure 1D). Preventing cohesin loading during S phase suppressed establishment of intra-chromosomal contacts (Figure S1B) and loop formation (Figure 1B, right panel) and the overall contacts displayed little changes compared to those observed in G1-arrested cells that contain little, if any, Scc1 (Figures S1A). Therefore, DNA loops and local contact enrichment observed along mitotic chromosomes are cohesin-dependent.

Because of the population average nature of Hi-C, the systematic presence of all these loops in each cell cannot be directly addressed here. However, to further characterize loops and to analyze whether they correspond to contacts between Scc1 enrichment sites

Verzijlbergen et al., 2014), we generated pile-up plots. Pile-up plots aim at depicting the average contact signal between pairs of Scc1 enrichment sites (Verzijlbergen et al., 2014). Briefly, for each condition, contacts between all pairs of 80 kb windows, centered on Scc1, and separated by 0 to 20 kb, were aggregated. A randomized set of windows separated by similar distances was also computed. The pile-up plot resulted from the ratio between the Scc1-centered aggregated maps and the randomized set. The same process was applied for pairs of cohesins enrichment sites separated by increasing distances, from 0 kb to 140 kb, with 20 kb steps (Figure 1E, Methods, (Gassler et al., 2017; Muller et al., 2018)). The color scale of the plots reflects the differences in contacts between the two aggregated maps: the redder, the more contacts are enriched on the maps centered on Scc1 enrichment sites. In metaphase, a strong dot signal appeared at the center of the pile-up, *i.e.* between pairs of cohesin-binding sites (Figure 1F, Methods), that vanishes over distances larger than 40 kb. These dots point as enriched contacts between pairs of discrete cohesin binding sites, e.g. loop-like structures. The strength of the dot signal can be assessed by dividing the median value of the central 3x3 square (i.e. the signal value), by the median of the top-right corner square (i.e. the background value). Pile-up plots confirm that the yeast mitotic chromosomes are organized into chromatin loops anchored at cohesin binding sites.

Peaks of cohesin enrichment sites overlap, on average, with convergent transcription sites (Busslinger et al., 2017; Glynn et al., 2004; Hu et al., 2015; Lengronne et al., 2004; Paldi et al., 2019). The basis of DNA loops, which involve such cohesin enriched regions, were indeed and unsurprisingly also found to be preferentially positioned within convergent genes (as illustrated in Figure S1C).

Cohesin dependent loops are independent of sister chromatid cohesion

Mitotic loops could arise from the bridging of cohesins involved in sister chromatid cohesion. To test this hypothesis, we generated Hi-C maps of mitotic chromosomes from cells depleted for Cdc45, which reach mitosis without replication (Tercero et al., 2000) (Figures 2A and S2A). Contact maps and their associated DNA loops (Figures 2B and S2B), $P_c(s)$ (Figures 2C and S2D) and pile-up plots of mitotic unreplicated and replicated cells showed little, if any, differences (Figure 2D). In addition, DNA loops of unreplicated mitotic chromosomes disappear in the absence of Scc1 (Figures 2B, 2C, 2D and S2C). Altogether, these results show that sister chromatid cohesion is not necessary for generating Scc1-dependent structures.

To further determine whether cohesin-mediated loops along mitotic chromosomes depend on a mitosis specific activity, we induced cohesin loading on unreplicated chromosomes in G1. An engineered version of Scc1 that cannot be cleaved by separase was induced in G1 arrested cells (Uhlmann et al., 2000) (Figures 3A and S3A) and contact maps were generated (Figure 3B). Loading of cohesin on G1 chromosomes led to an accumulation of loops between pairs of Scc1 binding sites (Figures 3B and 3C) and a significant increase in intra-chromosomal contacts (Figures 3D, S3B, S3C and S3D). In this condition, loops appeared slightly larger than in mitosis, suggesting that their expansion is constrained in metaphase-arrested cells (Figure 3C). Altogether those results demonstrate that the establishment of cohesin-mediated DNA loops along mitotic chromosomes is independent of sister-chromatid cohesion and of a mitosis specific activity.

Wpl1-mediated releasing activity counteracts loop expansion

In the absence of Wpl1, cohesins cannot be released from DNA. In mammals, Hi-C studies of WAPL-depleted cells revealed an enlargement of cohesin loops along interphase chromosomes which was interpreted as a hint of a loop extrusion process (Wutz et al., 2017).

To gain insights into the mechanism generating cohesin loops in yeast metaphase chromosomes, we therefore tested whether intra chromosomal contacts, $P_c(s)$ and DNA loops spread to greater distances in Wpl1-depleted cells. Wild-type and *wpl1Δ* cells were synchronized in metaphase by depleting Cdc20 (Figure S4A) and genome-wide chromatin interactions were quantified by Hi-C (Figure 4A). In Wpl1-depleted cells, the contact map displayed a very different pattern as compared to wild-type, with less short-range contacts overall (but a crispier constriction at the centromere level, clearly separating the two chromosome arms), as well as chromatin loops punctuating the map resulting in a grid-like dotty pattern (Figures 4A and S4B). The former positions of wild-type loops often displayed a weaker signal in the absence of Wpl1 as compared to wild-type cells. On the other hand, contacts between discrete, cohesin enriched sites now appeared enriched over longer distances, as shown by pile-up plots (up to ~130 kb in the absence of Wpl1 compared to ~<40 kb in wild type) (Figures 4B and S4D). The $P_c(s)$ also confirmed the decrease in short-range contacts and the enrichment over longer distances (Figures 4C and S4C).

The resulting grid-like loop pattern was often, but not always, stronger in chromosomal regions proximal to the centromeres. This may be due to high levels of cohesin loading at centromeric regions or due to the fact that the centromeric region represents a roadblock to cohesin progression. Similarly to wt metaphase cells, the basis of DNA loops in Wpl1 depleted cells involve enriched cohesion sites preferentially positioned within convergent genes (Figure S4E). The effects of Wpl1 depletion were further supported by performing the experiment in cells harboring *pds5-S81R*, an allele abolishing cohesin release even in presence of Wpl1 (Figure S4).

Expansion of DNA loops induced by Wpl1 depletion was not specific to mitosis, as it was also observed in G1-arrested cells expressing the non-cleavable version of Scc1 (Figure S5).

Our data therefore show that similarly to human cells, the size of yeast cohesin-dependent loops becomes deregulated in the absence of Wpl1, extending over much longer distances, though still involving hotspots of cohesin depositions. It suggests that yeast cohesin organizes mitotic chromosome presumably by loop extrusion, similarly to the mechanism proposed by others to explain establishment of DNA loops by cohesin during mammalian interphase.

Dual roles for Pds5 in DNA looping

As Wpl1 works with Pds5 to mediate "releasing activity" we tested how Pds5 contributes to DNA loop regulation. G1-arrested cells were depleted for Pds5 using the degron system, released into S-phase and arrested in metaphase (Figure S6A). Loss of both Pds5/Eco1-mediated Smc3-K113 acetylation (Figure 5A) and sister chromatid cohesion (Figure 5B) confirmed efficient Pds5 degradation. The contact map of Pds5-depleted cells was generated (Figure 5C) and compared to control (Figures 5C and S6B) and *wpl1Δ* cells (Figures 5C and S6C). Comparison of maps (Figure 5C) revealed that the absence of Pds5 increased the amount of long-range intra-chromosomal DNA contacts to a much higher extent than in *wpl1Δ* cells, as confirmed by log ratio between maps (Figures S6B and S6C) and $P_c(s)$ curves (Figures 5E and S6D).

A close inspection of Hi-C map also revealed that, as in metazoan (Wutz et al., 2017), Pds5 depletion induced a decrease in the number of discrete spots/DNA loops compared to wild-type and *wpl1Δ* cells (Figure 5C). While in wild-type and *wpl1Δ* cells, loops bridge discrete pairs of Scc1-enriched sequences, in Pds5-depleted cells loop bases were more loosely defined, with no clear-cut dots in the normalized Hi-C maps (Figure 5C). This was confirmed by pile-up plots showing that in Pds5 depleted cells, DNA loops did not

accumulate within those cohesin-rich loci as clearly as in wild-type cells (Figures 5D and S6E).

In metaphase-arrested Pds5-depleted cells, the insulation of peri-centromeric regions from the rest of chromosome arms was reduced. Whereas in wt and Wpl1-depleted cells the immediate left and right centromere-flanking regions appear to form a discrete "domain" (Figure S6F, see pink rectangle), this small structure disappears in the absence of Pds5. Instead, both regions now became able to engage in long-range contacts with their entire adjacent arm, up to the telomere. In addition, the ratio plot between Pds5-depleted and wild-type mitotic maps also showed a significant loss of contacts between the two arms (Figure S6B). As a result, each chromosome arm appears on the maps as a large self-interacting domain (Figure 5C).

To analyze whether pericentromeric, long-range contacts affect centromere clustering in the absence of Wpl1 or Pds5, we looked at the positioning of the fluorescently labelled Ndc80 kinetochore protein in the nuclei of nocodazole-arrested cells. Whereas in wild-type and Scc1-depleted cells all Ndc80 fluorescent signals appeared as two bright dots, both in *wpl1*Δ and Pds5-depleted cells this structure was accompanied by multiple, small discrete dots (Figure S6G). Given that the main difference between these different conditions consisted in the size of the loops, we propose that the engagement of each centromeric region in large loops induces a mechanical force promoting centromere de-clustering.

Chromosome contact patterns observed in Pds5-depleted cells suggest that Pds5 regulates loop formation not only *via* a Wpl1-mediated releasing activity, but also by an unknown, Wpl1-independent mechanism. As Pds5, but not Wpl1, is essential to maintain sister chromatid cohesion, we hypothesized that the increase in DNA loops sizes over longer distances in Pds5-depleted cells could result from loss of cohesion. Indeed, cohesins involved

285 in sister chromatid cohesion may act as physical barriers, or roadblocks, halting the loop
286 expansion process and defining loop basis positions along chromosomes. Inactivation of Pds5
287 would alleviate those discrete roadblocks, allowing loop expansion to proceed over longer
288 distances, and resulting in an increase in long-range contacts. To test this, we measured the
289 effects of Pds5 or Wpl1 loss on 3D folding of un-replicated (*cdc45*) chromosomes (Figures
290 6A, B and C). The depletion of either Wpl1 or Pds5 had the same effect on chromosome
291 structure than that observed in metaphase, with Pds5 inactivation leading to intra-
292 chromosomal contacts bridging loci over longer distances than in *wpl1Δ* cells, as illustrated
293 by log ratio between Hi-C maps (Figure 5F). Moreover, inactivation of Pds5 in Cdc45
294 depleted cells also induced a decrease in the number of discrete spots/DNA loops compared to
295 wild-type and *wpl1Δ* cells (Figures 6C and D).
296 Impact of Pds5 and Wpl1 depletion was also quantified in living cells: fluorescently-
297 labelled centromeres and a locus positioned 400 kb away on chromosome XV got closer
298 together compared to control cells (Figure 6E), backing the Hi-C results showing increased
299 loop sizes.
300 Those results therefore demonstrate that Pds5 regulates DNA contacts and suppresses
301 loop expansion through two mechanisms, the recruitment of Wpl1, as well as a Wpl1-
302 independent pathway.
303
304 ***Eco1 inhibits loop expansion***
305 Since increase in loop length in Pds5 depleted cells does not only result from the
306 absence of releasing activity, we envisioned that Pds5 recruitment of Eco1 (Chan et al., 2013;
307 Minamino et al., 2015; Noble et al., 2006; Vaur et al., 2012) might regulate a second
308 mechanism required to inhibit DNA loop expansion. We tested the effects of Eco1 depletion
309 using an inducible degron (Figures S7A and S7B; Methods) and showed that loss of Eco1 is

sufficient to result in spreading of contacts (Figures 7A, S7C and S7D) and loops (Figures 7A, C and S7F) to longer distances. As the absence of Eco1 promotes dissociation of cohesin from DNA by Wpl1 (Chan et al., 2012), these longer loops cannot result from an increase in cohesin residence time on DNA. Therefore, this result shows that in addition to promoting sister chromatid cohesion, Eco1 also inhibits the translocation process extending DNA loops. Remarkably, loop length (Figure 7A, C and S7F), contact probability ($P_c(s)$) (Figures 7B and S7B) and centromere clustering defects in Eco1 depleted cells (Figure S7G) were comparable to those observed in Wpl1 depleted cells, despite Eco1 and Wpl1 having opposing effects on releasing.

Since Pds5 recruits both Eco1 and Wpl1 on cohesin, we tested whether their co-inactivation would mimic the effect of Pds5 depletion. Indeed, depletion of Eco1 in *wpl1*Δ cells promoted long-range intra-chromosomal contacts and DNA loops nearly identical to those observed in Pds5 depleted cells (Figures 7, S7B, D and E). This suggests that the positioning of loop basis (hence the size of the loops) is regulated through two independent pathways, Eco1 and Wpl1.

DISCUSSION

In the present study, we show that yeast mitotic chromosomes organize into loops along individual chromatids, independently of replication. These loops are enriched in cohesin subunits at their basis. The cohesin binding factors Pds5, Wpl1 and Eco1 affect the sizes and distribution of these loops, with Pds5 regulating loop size *via* two pathways: the Wpl1-mediated releasing activity and an Eco1-dependent mechanism (Figure 7).

Yeast mitotic chromosomes are organized into cohesin-dependent loops

We show that DNA loops are present along yeast mitotic chromosomes. The bases of these loops are enriched in cohesin. Whether all cohesin deposition sites identified by chromatin immunoprecipitation followed by deep sequencing (ChIP-seq) are involved in loop formation in all cells, or whether a loop heterogeneity exists within the population remains to be characterized. Cohesin enrichment sites, and the bases of DNA loops in *wt* or Wpl1 depleted cells, correspond mostly to site of convergent genes. It has been proposed that accumulation of cohesin at these genomic positions may be driven by transcription (Lengronne et al., 2004). RNA polymerases along convergent genes may indeed represent boundaries or roadblocks to cohesin-dependent loop expansion, resulting in an accumulation of cohesin-dependent loop basis at sites of convergent transcription. We also noticed that Pds5 is crucial to maintain accumulation of cohesin-dependent loop at those sites. This implies that in absence of Pds5 the loop formation mechanism somehow manages to bypass the roadblocks.

Cohesin binding factors regulate loops expansion

It has been proposed that cohesin could promote chromatin loops formation *via* a loop extrusion mechanism (Fudenberg et al., 2016; Goloborodko et al., 2016; Nasmyth, 2001). This model predicts that the length of DNA loops should be dependent on cohesin residence time on DNA. Since Wpl1 inactivation increases cohesin's residence time on DNA, cohesin would extrude longer DNA in Wpl1-depleted cells. Indeed, Hi-C studies in mammals revealed an enlargement of cohesin-mediated loops along chromosomes in WAPL1-depleted cells. Our present study shows that the inactivation of Wpl1-mediated releasing also induces enlargement of DNA loops in *S. cerevisiae*. By analogy with mammals, we propose that this enlargement of DNA loops is the consequence of an increase of cohesin's residence time on DNA and that cohesin structure yeast mitotic chromosomes through a loop extrusion process.

Alternatively, one can envision another hypothesis whereby the longer range contacts observed in Wpl1-depleted cells result from cohesin loading defects due to Wpl1 depletion (Rowland et al., 2009). Indeed, the inactivation of Wpl1 could reduce the amount of cohesin being loaded on the chromatin, hence decreasing the number of complexes expanding DNA loops present along a chromosome arm. The lower density of cohesin may in turn lead to longer DNA tracks being transformed into loops by the same complex before colliding into another complex, and thus resulting in the formation of longer loops on average. Future works will determine whether loop enlargement in Wpl1-depleted cells is the consequence of cohesin loading defects, of an increase in cohesin's residence time on DNA, or both.

We also analyzed the role of other cohesin binding factors on loop structures and found that Pds5 regulates loop expansion *via* at least two pathways: the previously described Wpl1-mediated releasing activity (Wutz et al., 2017) and a novel Eco1-dependent mechanism (Figure 7). Our results point at a role of Eco1 in negatively regulating loop expansion through a mechanism independent of cohesion establishment. In agreement with our result a recent study reported that ESCO1 (human ortholog of Eco1) also inhibits the ability of cohesin to form long DNA loops (Wutz et al., 2019).

Competition between Scc2 and Pds5 may regulate DNA loop expansion

One may envision that Eco1-mediated acetylation inhibits translocase activity that expands cohesin-dependent loops. It has been proposed that ATP hydrolysis stimulated by Scc2 could be the driving force for loop expansion. As Pds5 competes with Scc2 for binding the kleisin subunit (Petela et al., 2018), a possibility is that Pds5 inhibits the translocation process required to expand DNA loops. Eco1-mediated acetylation may therefore improve Pds5 binding on cohesin and consequently abolish the Scc2-mediated translocation process. This idea is reinforced by *in vivo* FRAP measurements revealing that Eco1 inactivation

increases Pds5 turnover on chromosomes (Chan et al., 2013). Moreover, recent ChIP-seq data show that Eco1 inactivation reduces Pds5 association with DNA while it has no effect on cohesin ring association with DNA (Chapard et al., 2019).

Competition between Pds5 and Scc2 may also control loop expansion and cohesin positioning in human cells. This hypothesis is supported by the fact that Scc2 does not co-localize with CTCF which halts loop expansion. Wutz et al. (2017) showed that the ability of CTCF to block loop extrusion is dependent on PDS5. As discussed by the authors, replacement of Pds5 by Scc2 may be somehow inhibited at CTCF sites, which may consequently abolish or decrease the rate of ATPase hydrolysis required to expand DNA loops (Wutz et al., 2017).

How does Eco1 regulate competition between Scc2 and Pds5 during establishment and maintenance of cohesin-dependent loops? It may involve Eco1-mediated Smc3 acetylation as this reaction affects how Scc2 promotes loading of cohesin onto DNA (Hu et al 2015). However, additional investigations are necessary to determine whether Smc3 acetylation is involved in regulation of DNA loops. Deciphering how Eco1 influences DNA loop expansion may provide new perspectives to understand how human Eco1 homologues (ESCO1 and ESCO2) regulate gene transcription or how they deficiency induces the developmental disorder called Roberts syndrome.

DNA looping is blocked at centromeres

Our study points out that the yeast centromere is a strong roadblock to cohesin-dependent loop expansion. The nature of this boundary raises interests beyond the yeast community, as related mechanisms could apply in other species as well. In yeast, kinetochore proteins bound to centromeres are connected through microtubules to the MTOC (spindle pole body or SPB) which itself is embedded in the nuclear envelope. Such a physical bridge

could block the progression of incoming cohesin along the chromosome. It is also possible that the huge kinetochore complex bound to centromeres is sufficient to stop DNA loop expansion.

In wild type cells, Wpl1 mediates cohesin release and Eco1 restricts DNA loop progression from chromosome arms to centromeric regions. When those activities are impaired, loops emanating from chromosome arms can extend to centromeres, but no further, resulting in sharp, discrete boundaries as observed on the contact maps. In addition, it is likely that loops also originate from centromeres and spread towards chromosome arms.

Finally, we showed that centromere clustering is impaired in Wpl1, Pds5 or Eco1 depleted cells (Figure S6G and S7G). This suggests that centromere clustering is exposed to opposite forces emanating from microtubules and, presumably, a loop extrusion-like mechanism that promote loop expansion. Inhibiting such loop extruding mechanism in wild-type cells may favor the insulation of clustered centromeres away from chromosome arms, and consequently improve or stabilize microtubule attachment and chromosome segregation. It remains to be investigated whether similar mechanisms occur in species with larger and epigenetically defined centromeres compared to the budding yeast point centromere, and whether the attachment of microtubules is mandatory to bock DNA looping.

Acknowledgements

We thank T.U. Tanaka and K. Nasmyth for sharing strains and K. Shiahige for the Smc3 antibody. We thank Aurèle Piazza, Luis Aragon, Julien Mozziconacci, Christophe Chapard, Olivier Cuvier, Tony Marchal, and OG and RK teams for discussions and comments on the manuscript. LD was supported by ARC fellowships. This research was supported by funding to R.K. from the European Research Council under the Horizon 2020 Program (ERC grant agreement 260822).

Author contributions

LD, RK and FB designed research. LD and AT performed the experiments, with help from LLS who initiated the study. RM analyzed the data, with contributions from AC. All authors interpreted the data. LD, RK, FB wrote the manuscript, with contributions from RM.

Declaration of interest

The authors declare no competing interests.

Data Availability

Sample description and raw sequences are accessible on SRA database through the following accession number: PRJNA528616.

Figure Legends

Figure 1. Mitotic yeast chromosomes are organized as cohesin-dependent loops and domains. A) Left panel: schematic representation of the experimental protocol used to process cells from G1 to metaphase in absence or presence of Scc1 (strains FB133-57B and yLD127-20b). Right panel: cell-cycle arrest monitored by flow cytometry. Percentage of bi-nucleated (anaphase) cells was measured to evaluate the efficiency of the metaphase arrest. B) Contact maps of a part of chromosome IV (1 kb bin) for control and Scc1-depleted, metaphase-arrested strains (strains FB133-57B and yLD127-20b) and G1 arrested cells (strain FB09-9C), Scc1 ChIp seq profile and chromosomal contact along 100kb region of chromosome IV are shown in the black square. C) Derivative of the curve plotting contact probability as a function of genomic distance (log scale). D) Percentage of cells with paired or unpaired fluorescently labelled URA3 loci (ura3::3xURA3 tetO112; tetR-GFP), carrying or not a Scc1-AID degron (strains yLD126-36c and FB124), in presence of auxin. Scale bar, 2 μm. E) Schematic representation of the analysis pipeline used to generate pile-up ratio plots. F) Pile-up ratio plots of 80 kb windows (2 kb bin) centered on pairs of Scc1-enriched or randomly chosen positions (Methods). Ratios are ordered according to the distance between Scc1 enriched positions. Blue color: more contacts between the random genomic regions. Red signal: more contacts between Scc1-enriched regions. The italic numbers atop each pile-up reflect the strength of the central signal compared to background (Methods). See also Figure S1.

Figure 2. Cohesin-dependent loops and domains on mitotic yeast chromosomes are independent of sister chromatid cohesion. A) Schematic representation of the experimental protocol used to generate unreplicated mitotic cells in absence or presence of Scc1 (strains FB154 and FB149- 11B). B) Contact maps of a part of chromosome IV (1 kb bin) for

unreplicated mitotic cells (*cdc45*) with or without Scc1 (strains FB154 and FB149-11B) and for metaphase-arrested cells (*cdc20*, strain FB133-57B). C) Derivative of the curve plotting contact probability as a function of genomic distance (log scale). D) Pile-up ratio plots of 80 kb windows (2 kb bin) centered on pairs of Scc1-enriched or randomly chosen positions (see Figure 1F). See also Figure S2.

Figure 3. Expression of Scc1 in G1-arrested cells induces DNA looping. A) Left panel: Schematic representation of the experimental protocol followed to overexpress a HA-tagged, non-cleavable Scc1 in G1. Right panel: western blot assessing expression of non-cleavable Scc1 (*OE scc1*) with anti-HA antibody and expression of endogenous Scc1 (Scc1-PK) with anti-V5 antibody. B) Contact maps of a part of chromosome IV (1 kb bin) for G1-arrested cells with or without Scc1 (strains FB09-9C and FB09-4A) and for metaphase-arrested strain (*cdc20*, FB133-57B). C) Pile-up ratio plots of 80 kb windows (2 kb bin) centered on pairs of Scc1-enriched or randomly chosen positions (see Figure 1F). D) Derivative of the curve plotting contact probability as a function of genomic distance. Black digits reflect the strength of the central signal compared to background. See also Figure S3.

Figure 4. Wpl1 restricts DNA loop expansion. A) Contact maps of a part of chromosome IV (1 kb bin) of wild type and *wpl1*Δ strains arrested in metaphase (strains FB133-57B and FB133-49B). B) Pile-up ratio plots of 80 kb windows (2 kb bin) centered on pairs of Scc1-enriched or randomly chosen positions (see Figure 1F). C) Derivative of the curve plotting contact probability as a function of genomic distance. See also Figure S4 and S5.

Figure 5. A Wpl1-independent pathway regulates cohesin-dependent loops during mitosis. A) Pds5 depletion was monitored by western blot through the Pds5-dependent acetylation of

Smc3-K113. Pgk1, loading control. B) Sister-chromatid cohesion was monitored by detecting paired/unpaired fluorescently labelled URA3 loci in presence or absence of Pds5 (strains yLD126-36c and yLD126-38b). Scale bar, 2 μm. C) Hi-C contact maps of metaphase-arrested cells in presence or absence of Pds5 or Wpl1 (1 kb bin). Chromosomes X and XI are represented with pink and green lines, respectively. D) Pile-up ratio plots of 80 kb windows (2 kb bin) centered on contacts between pairs of Scc1-enriched or randomly chosen positions (see Figure 1F). E) Derivative of the curve plotting contact probability as a function of genomic distance (log scale) for metaphase arrested strains. F) Log2 ratio between Hi-C maps from metaphase-arrested strains or Cdc45-depleted cells expressing or not Wpl1 or Pds5 (1 kb bin). Blue to red color scale reflects the enrichment in contacts in one population with respect to the other. See also Figure S6.

Figure 6. Effect of Pds5 or Wpl1 loss on the 3D folding of un-replicated mitotic chromosomes. A) Unreplicated mitotic cells without Pds5 or Wpl1 were generated with strains FB154 (control), FB148-3C (*wpl1Δ*) and FB156-5a (*pds5-AID*). Cell cycle was monitored by flow cytometry. Percentage of bi-nucleated (anaphase) cells and budding indexes were measured. B) Derivative of the curve plotting contact probability as a function of genomic distance (log scale). C) Hi-C contact maps of unreplicated mitotic cells in absence of Pds5 or Wpl1 (1 kb bin). D) Pile-up ratio plots of 80 kb windows (2 kb bin) centered on contacts between pairs of Scc1-enriched or randomly chosen positions (see Figure 1F). E) Fluorescent imaging of strains yLD162-13a (control), yLD162-2b (*wpl1*Δ) and yLD163-22a (*pds5-AID*) strains harboring fluorescently labelled kinetochores (Ndc80-GFP) and HIS3 gene (TetO/TetR-mRFP, 400 kb away from the chromosome XV centromere). Cells were arrested in early S phase by expressing a non-degradable version of Sic1 protein. Scale bar, 2 μm.

Distances between kinetochores and the HIS3 locus were measured in each condition and plotted as cumulative distributive functions. See also Figure S7.

Figure 7. Eco1 counteracts loop expansion. A) Hi-C maps (1 kb bin) for strains FB133- 57B (wild-type), FB133-20C (*eco1-AID*), FB133-49B (*wpl1Δ*) and FB133-1D (*wpl1Δ eco1-AID*) and yLD121-1a (*pds5-AID*) arrested in metaphase. The chromosomes are indicated for each map. B) Derivative of the curve plotting contact probability as a function of genomic distance (log scale) for metaphase arrested strains. C) Pile-up ratio plots of 80 kb windows (2 kb bin) centered on pairs of Scc1-enriched or randomly chosen positions (see Figure 1F). D) Model showing the two Pds5-regulated pathways inhibiting DNA loop expansion through a loop extrusion mechanism. Left: Eco1 inhibits cohesin translocase activity; right: Wpl1 opens the Smc3-Scc1 gate and dissociates cohesin from DNA.

STAR METHODS

LEAD CONTACT AND MATERIALS AVAILABILITY

Further information and requests for resources and reagents should be directed to and will be fulfilled by the Lead Contact, Romain Koszul (romain.koszul@pasteur.fr)

EXPERIMENTAL MODEL AND SUBJECT DETAILS

Yeast Strains and Plasmids

All strains are derivatives of W303. Strains and plasmids are listed in Key Resources Table and in Supplementary Table S2

Media and growth conditions

Strain yLD118-1a (MET3-CDC20) was grown overnight at 30°C in 150ml of synthetic complete medium deprived of methionine (SC-Met) (SC: 0.67% yeast nitrogen base without amino acids (Difco)), supplemented with a mix of amino-acids, uracil and adenine, 2% glucose) to reach 4,2 x 10^8 cells. To induce metaphase arrest, cells were arrested in G1 for 2h30 by addition of alpha-factor (Antibody-online, ABIN399114) every 30min (1µg/ml final), washed 3 times and released in rich medium (YPD: 1% bacto peptone (Difco), 1% bacto yeast extract (Difco) and 2% glucose) supplemented with methionine (2mM final). 2h latter cells were fixed for Hi-C. Strains yLD127-20b, yLD121-1a, FB133-57B, FB133-20C, FB133-49B, FB133-1D were processed as described above except auxin addition (Sigma-Aldrich, I3750) (1mM final) to the media 1h after starting alpha-factor treatment. Cells were released from G1 in YPD supplemented with methionine and auxin (1mM final). Strains FB08-5C, FB08-6A, FB09-4A, FB09-9C were grown overnight in 300ml of YP medium

supplemented with raffinose 2% (Sigma-Aldrich, R0250) to reach 8,4 x 10^8 cells. Expression of Scc1(R180D,268D)-HA was induced 1h after starting alpha-factor treatment by addition of newly-made galactose (Sigma-Aldrich, G0750) (2% final) to the cultures. Cells were fixed for Hi-C after 2h30 in alpha-factor. Strains FB154, FB149-11B, FB148-3C, FB156-5a (CDC45-AID) were grown overnight in 150ml YPD to reach 4,2 x 10^8 cells. G1 arrest and auxin addition were conducted as previously, (except auxin concentration, 2mM final), cells were released in YPD media supplemented with auxin (2mM final) for 80min and fixed for Hi-C.

METHOD DETAILS

Flow cytometry

About 2,8 x 10^6 were fixed in ethanol 70% and stored at -20°C. Cells were the pelleted, washed and incubated overnight in Tris-HCl 50mM pH 7,5 complemented with RNase A (10 mg/ml; Sigma-Aldrich) at 37°C. Cells were pelleted, resuspended 400µl of 1,0mg/ml propidium iodide (Fisher, P3566) in 50mM Tris pH 7,4, NaCl, MgCl2 and incubated for 1 h at room temperature. Flow cytometry was performed on a CyFlow® ML Analyzer (Partec) and data were analyzed using FloMax software.

Microscopy

Strains FB124, yLD126-38b, yLD126-36c were grown overnight in SC-Met at 30°C. The next day cells were diluted in fresh media. Exponentially growing cells were arrested in G1 with alpha-factor treatment, induced with auxin (1mM final), washed and arrested in metaphase as described above. Strains yLD162-13a, yLD162-2b, yLD163-22a were grown overnight in YP-raffinose at 30°C. The next day, after dilution in fresh media, exponentially growing cells were arrested in G1 with alpha-factor treatment and while being induced with

auxin (1mM final). Expression of non-degradable Sic1 was induced 30min before release by addition of galactose (2% final) to the media. Cells were washed and released in YP supplemented with raffinose and galactose for 120min. Cells were placed on 2% agarose pads made of synthetic complete medium plus glucose. Live cell imaging was performed under a spinning disk confocal system (Nipkow Revolution, Andor Technology) with an EM charge-coupled device (CCD) camera (DU 888; Andor Technology) mounted on an inverted microscope (IX-81; Olympus) featuring a CSU22 confocal spinning disk unit (Yokogawa Corporation of America). Image acquisition was done at 30°C. 41 Z-stacking images with 0.25µm intervals were acquired by using IQ2 software with 200ms exposure time. Were used: 100× objective lens (Plan-Apochromat, 1.4 NA, oil immersion; Olympus) and single laser lines for excitation, diode pumped solid state lasers (DPSSL). GFP fluorescence was excited at 488 nm (50 mW; Coherent) and mCherry fluorescence at 561 nm (50 mW; Cobolt jive). Green and red fluorescence were collected using a bi-bandpass emission filter (Em01-R488/568-15; Semrock). Pixel were 65nm in size.

Acetylation assays

A pellet from 10^7 cells was frozen in liquid nitrogen and stored at −20°C overnight. The cell pellet was resuspended in 100µl H20, 20µl trichloroacetic acid (Sigma-Aldrich, T8657) and broken with glass beads at 4°C. Precipitated proteins were resuspended in Laemmly buffer/ Tris HCl pH 8,0 and extracted by cycles of 5min heating at 80°C- 5min vortexing at 4°C. Eluates were analyzed by SDS-PAGE followed by western blotting with antibodies anti-V5 tag (VWR, MEDMMM-0168-P), anti-Pgk1 (Invitrogen, 459250) and anti-Smc3-K113Ac (Beckouët et al., 2010).

Hi-C libraries

Hi-C was performed as described (Lazar-Stefanita et al., 2017), except cells were disrupted using a Precellys apparatus (Bertin Instruments) instead of processed through zymolyase treatment. Aliquots of 1-3 x 10^9 cells in 150 ml YPD/synthetic medium were fixed in 3% formaldehyde (Sigma, F8775) for 20 min at room temperature and quenched with 25 ml glycine 2.5 M for 20 min at 4°C. Cross-linked cells were recovered through centrifugation, washed with YPD and a 150 mg pellet was stored at -80°C. Hi-C DNA libraries were 500 bp sheared using CovarisS220 apparatus, and the biotin-labeled fragments were selectively captured by Dynabeads Myone Streptavidin C1 (Invitrogen). The resulting libraries were used as template for the llumina amplification by PE-PCR primers and paired-end sequenced on a NextSeq500 Illumina platform. All Hi-C libraries are listed in Supplementary Table 1.

QUANTIFICATION AND STATISTICAL ANALYSIS

Processing of the reads and generation of contact maps

Pairs of reads were aligned independently using Bowtie2 in its most sensitive mode against the latest *S. cerevisiae* W303 reference genome (GCA_002163515.1), corrected for a chromosomal inversion on chromosome 16 revealed by the Hi-C data. Alignment was done using an iterative procedure and each uniquely mapped read was assigned to a restriction fragment. Uncuts, loops and religation events were filtered as described (Cournac et al., 2012). Contact matrices were built with resolutions of 2 or 20kb (bin sizes) and normalized using the sequential component procedure (Cournac et al., 2012). Log-ratios were generated by dividing 2 normalized contact maps, with the same resolution, by one another and then computing the log2 of the resulting matrix.

Computation of the contact probability as a function of genomic distance

Contact probability as a function of genomic distance $P_c(s)$ was determined as described (Muller et al., 2018). Intra-chromosomal pairs of reads were selected and partitioned by chromosome arms. Pairs oriented towards different directions or separated by less than 1.5 kb were discarded. For each chromosome, the remaining pairs were log-binned as a function of their genomic distance s using the formula: bin = [log1.1(s)]. The number of read pairs in each bin was counted and weighed by the bin size 1.1(1+bin), as well as the difference between the length of the chromosome and the genomic distance.

Identification of cohesin binding-sites and generation of pile-up plots

Data from (Verzijlbergen et al., 2014) were used to generate Scc1 ChIP-Seq profiles with a 2kb resolution. Bins with a signal over 1.5 were labelled as cohesin binding sites (CBS). CBS were determined for wild type and Pds5-AID (Petela et al., 2018) strains. All possible pairs of CBS within chromosomal arms were determined and partitioned according to their genomic distance. In 2kb resolution contact maps, windows surrounding these positions were extracted and averaged. The resulting observed signal was divided by the expected signal, generated by averaging the windows around random positions having the same genomic distance as the pairs of CBS. For each window, undercovered bins were defined as bins with a total number of reads under *median (number of reads / bin) – SD* and excluded of the averaging operations to reduce noise. The strength of the central (loop) signal was assessed by dividing the median value of the central 3x3 square (i.e. the signal value), by the median of the top-right corner square (i.e. the background value). As a consequence, the more “loop signal”, the higher the score (> 1). Since loops will deplete longer range contacts, a strong loop signal will be accompanied at longer distances by a weak one (< 1). No loops will result in a signal ~1. See Flyamer et al., 2019, for a similar approach.

DATA AND CODE AVAILABILITY

Sample description and raw sequences are accessible on SRA database through the following accession number: PRJNA528616.

Codes and functions used to generate the figures from the raw data are available online (https://github.com/koszullab/hicstuff).

Imaging data are available on Mendeley (https://data.mendeley.com/datasets) under the DOI: 10.17632/pgwsf28v2d.

Bibliography

Beckouët, F., Hu, B., Roig, M.B., Sutani, T., Komata, M., Uluocak, P., Katis, V.L., Shirahige, K., and Nasmyth, K. (2010). An Smc3 acetylation cycle is essential for establishment of sister chromatid cohesion. Mol. Cell *39*, 689–699.

Beckouët, F., Srinivasan, M., Roig, M.B., Chan, K.-L., Scheinost, J.C., Batty, P., Hu, B., Petela, N., Gligoris, T., Smith, A.C., et al. (2016). Releasing activity disengages cohesin's smc3/scc1 interface in a process blocked by acetylation. Mol. Cell *61*, 563–574.

Busslinger, G.A., Stocsits, R.R., van der Lelij, P., Axelsson, E., Tedeschi, A., Galjart, N., and Peters, J.-M. (2017). Cohesin is positioned in mammalian genomes by transcription, CTCF and Wapl. Nature *544*, 503–507.

Cavalli, G., and Misteli, T. (2013). Functional implications of genome topology. Nat. Struct. Mol. Biol. *20*, 290–299.

Chan, K.-L., Roig, M.B., Hu, B., Beckouët, F., Metson, J., and Nasmyth, K. (2012). Cohesin's DNA exit gate is distinct from its entrance gate and is regulated by acetylation. Cell *150*, 961–974.

Chan, K.-L., Gligoris, T., Upcher, W., Kato, Y., Shirahige, K., Nasmyth, K., and Beckouët, F. (2013). Pds5 promotes and protects cohesin acetylation. Proc. Natl. Acad. Sci. USA *110*, 13020–13025.

Chapard, C., Jones, R., van Oepen, T., Scheinost, J.C., and Nasmyth, K. (2019). Sister DNA Entrapment between Juxtaposed Smc Heads and Kleisin of the Cohesin Complex. Mol. Cell.

Ciosk, R., Shirayama, M., Shevchenko, A., Tanaka, T., Toth, A., Shevchenko, A., and Nasmyth, K. (2000). Cohesin's binding to chromosomes depends on a separate complex consisting of Scc2 and Scc4 proteins. Mol. Cell *5*, 243–254.

Cournac, A., Marie-Nelly, H., Marbouty, M., Koszul, R., and Mozziconacci, J. (2012). Normalization of a chromosomal contact map. BMC Genomics 13, 436.

Dauban, L., Kamgoue, A., Wang, R., Léger-Silvestre, I., Beckouët, F., Cantaloube, S., and Gadal, O. (2019). Quantification of the dynamic behaviour of ribosomal DNA genes and nucleolus during yeast Saccharomyces cerevisiae cell cycle. J. Struct. Biol.

Dekker, J., and Mirny, L. (2016). The 3D genome as moderator of chromosomal communication. Cell *164*, 1110–1121.

Dekker, J., Rippe, K., Dekker, M., and Kleckner, N. (2002). Capturing chromosome conformation. Science *295*, 1306–1311.

Fudenberg, G., Imakaev, M., Lu, C., Goloborodko, A., Abdennur, N., and Mirny, L.A.

(2016). Formation of chromosomal domains by loop extrusion. Cell Rep. *15*, 2038–2049.

Flyamer, I.M., Illingwirth, R.S., and Bickmore, W.A. (2019). *Coolpup.py: versatile pile-up analysis of Hi-C data*. Biorxiv doi: https://doi.org/10.1101/586537

Gandhi, R., Gillespie, P.J., and Hirano, T. (2006). Human Wapl is a cohesin-binding protein that promotes sister-chromatid resolution in mitotic prophase. Curr. Biol. *16*, 2406–2417.

Ganji, M., Shaltiel, I.A., Bisht, S., Kim, E., Kalichava, A., Haering, C.H., and Dekker, C. (2018). Real-time imaging of DNA loop extrusion by condensin. Science *360*, 102–105.

Gassler, J., Brandão, H.B., Imakaev, M., Flyamer, I.M., Ladstätter, S., Bickmore, W.A., Peters, J.-M., Mirny, L.A., and Tachibana, K. (2017). A mechanism of cohesin-dependent loop extrusion organizes zygotic genome architecture. EMBO J. *36*, 3600–3618.

Gibcus, J.H., Samejima, K., Goloborodko, A., Samejima, I., Naumova, N., Nuebler, J., Kanemaki, M.T., Xie, L., Paulson, J.R., Earnshaw, W.C., et al. (2018). A pathway for mitotic chromosome formation. Science *359*.

Gligoris, T.G., Scheinost, J.C., Bürmann, F., Petela, N., Chan, K.-L., Uluocak, P., Beckouët, F., Gruber, S., Nasmyth, K., and Löwe, J. (2014). Closing the cohesin ring: structure and function of its Smc3-kleisin interface. Science *346*, 963–967.

Glynn, E.F., Megee, P.C., Yu, H.-G., Mistrot, C., Unal, E., Koshland, D.E., DeRisi, J.L., and Gerton, J.L. (2004). Genome-wide mapping of the cohesin complex in the yeast Saccharomyces cerevisiae. PLoS Biol. *2*, E259.

Goloborodko, A., Marko, J.F., and Mirny, L.A. (2016). Chromosome compaction by active loop extrusion. Biophys. J. *110*, 2162–2168.

Guacci, V., Hogan, E., and Koshland, D. (1994). Chromosome condensation and sister chromatid pairing in budding yeast. J. Cell Biol. *125*, 517–530.

Haarhuis, J.H., and Rowland, B.D. (2017). Cohesin: building loops, but not compartments. EMBO J. *36*, 3549–3551.

Haering, C.H., Löwe, J., Hochwagen, A., and Nasmyth, K. (2002). Molecular architecture of SMC proteins and the yeast cohesin complex. Mol. Cell *9*, 773–788.

Haering, C.H., Farcas, A.-M., Arumugam, P., Metson, J., and Nasmyth, K. (2008). The cohesin ring concatenates sister DNA molecules. Nature *454*, 297–301.

Hu, B., Itoh, T., Mishra, A., Katoh, Y., Chan, K.-L., Upcher, W., Godlee, C., Roig, M.B., Shirahige, K., and Nasmyth, K. (2011). ATP hydrolysis is required for relocating cohesin from sites occupied by its Scc2/4 loading complex. Curr. Biol. *21*, 12–24.

Hu, B., Petela, N., Kurze, A., Chan, K.-L., Chapard, C., and Nasmyth, K. (2015).

736 Biological chromodynamics: a general method for measuring protein occupancy across the
737 genome by calibrating ChIP-seq. Nucleic Acids Res. *43*, e132.
738 Kagey, M.H., Newman, J.J., Bilodeau, S., Zhan, Y., Orlando, D.A., van Berkum, N.L.,
739 Ebmeier, C.C., Goossens, J., Rahl, P.B., Levine, S.S., et al. (2010). Mediator and cohesin
740 connect gene expression and chromatin architecture. Nature *467*, 430–435.
741 Kueng, S., Hegemann, B., Peters, B.H., Lipp, J.J., Schleiffer, A., Mechtler, K., and Peters,
742 J.-M. (2006). Wapl controls the dynamic association of cohesin with chromatin. Cell *127*,
743 955–967.
744 Lazar-Stefanita, L., Scolari, V.F., Mercy, G., Muller, H., Guérin, T.M., Thierry, A.,
745 Mozziconacci, J., and Koszul, R. (2017). Cohesins and condensins orchestrate the 4D
746 dynamics of yeast chromosomes during the cell cycle. EMBO J. *36*, 2684–2697.
747 Le, T.B.K., Imakaev, M.V., Mirny, L.A., and Laub, M.T. (2013). High-resolution mapping
748 of the spatial organization of a bacterial chromosome. Science *342*, 731–734.
749 Lengronne, A., Katou, Y., Mori, S., Yokobayashi, S., Kelly, G.P., Itoh, T., Watanabe, Y.,
750 Shirahige, K., and Uhlmann, F. (2004). Cohesin relocation from sites of chromosomal loading
751 to places of convergent transcription. Nature *430*, 573–578.
752 Liang, Z., Zickler, D., Prentiss, M., Chang, F.S., Witz, G., Maeshima, K., and Kleckner, N.
753 (2015). Chromosomes progress to metaphase in multiple discrete steps via global
754 compaction/expansion cycles. Cell *161*, 1124–1137.
755 Lioy, V.S., Cournac, A., Marbouty, M., Duigou, S., Mozziconacci, J., Espéli, O., Boccard,
756 F., and Koszul, R. (2018). Multiscale Structuring of the E. coli Chromosome by Nucleoid-
757 Associated and Condensin Proteins. Cell *172*, 771–783.e18.
758 Marbouty, M., Le Gall, A., Cattoni, D.I., Cournac, A., Koh, A., Fiche, J.-B.,
759 Mozziconacci, J., Murray, H., Koszul, R., and Nollmann, M. (2015). Condensin- and
760 Replication-Mediated Bacterial Chromosome Folding and Origin Condensation Revealed by
761 Hi-C and Super-resolution Imaging. Mol. Cell *59*, 588–602.
762 Minamino, M., Ishibashi, M., Nakato, R., Akiyama, K., Tanaka, H., Kato, Y., Negishi, L.,
763 Hirota, T., Sutani, T., Bando, M., et al. (2015). Esco1 Acetylates Cohesin via a Mechanism
764 Different from That of Esco2. Curr. Biol. *25*, 1694–1706.
765 Mizuguchi, T., Fudenberg, G., Mehta, S., Belton, J.-M., Taneja, N., Folco, H.D.,
766 FitzGerald, P., Dekker, J., Mirny, L., Barrowman, J., et al. (2014). Cohesin-dependent
767 globules and heterochromatin shape 3D genome architecture in S. pombe. Nature *516*, 432–
768 435.
769 Muller, H., Scolari, V.F., Agier, N., Piazza, A., Thierry, A., Mercy, G., Descorps-Declere,

S., Lazar-Stefanita, L., Espeli, O., Llorente, B., et al. (2018). Characterizing meiotic chromosomes' structure and pairing using a designer sequence optimized for Hi-C. Mol. Syst. Biol. *14*, e8293.

Murayama, Y., and Uhlmann, F. (2015). DNA Entry into and Exit out of the Cohesin Ring by an Interlocking Gate Mechanism. Cell *163*, 1628–1640.

Nasmyth, K. (2001). Disseminating the genome: joining, resolving, and separating sister chromatids during mitosis and meiosis. Annu. Rev. Genet. *35*, 673–745.

Nasmyth, K., and Haering, C.H. (2009). Cohesin: its roles and mechanisms. Annu. Rev. Genet. *43*, 525–558.

Noble, D., Kenna, M.A., Dix, M., Skibbens, R.V., Unal, E., and Guacci, V. (2006). Intersection between the regulators of sister chromatid cohesion establishment and maintenance in budding yeast indicates a multi-step mechanism. Cell Cycle *5*, 2528–2536.

Nora, E.P., Goloborodko, A., Valton, A.-L., Gibcus, J.H., Uebersohn, A., Abdennur, N., Dekker, J., Mirny, L.A., and Bruneau, B.G. (2017). Targeted Degradation of CTCF Decouples Local Insulation of Chromosome Domains from Genomic Compartmentalization. Cell *169*, 930–944.e22.

Paldi, F., Alver, B., Robertson, D., Schalbetter, S.A., Kerr, A., Kelly, D.A., Neale, M.J., Baxter, J., and Marston, A.L. (2019). Convergent genes shape budding yeast pericentromeres. BioRxiv.

Parelho, V., Hadjur, S., Spivakov, M., Leleu, M., Sauer, S., Gregson, H.C., Jarmuz, A., Canzonetta, C., Webster, Z., Nesterova, T., et al. (2008). Cohesins functionally associate with CTCF on mammalian chromosome arms. Cell *132*, 422–433.

Petela, N.J., Gligoris, T.G., Metson, J., Lee, B.-G., Voulgaris, M., Hu, B., Kikuchi, S., Chapard, C., Chen, W., Rajendra, E., et al. (2018). Scc2 Is a Potent Activator of Cohesin's ATPase that Promotes Loading by Binding Scc1 without Pds5. Mol. Cell *70*, 1134–1148.e7.

Rolef Ben-Shahar, T., Heeger, S., Lehane, C., East, P., Flynn, H., Skehel, M., and Uhlmann, F. (2008). Eco1-dependent cohesin acetylation during establishment of sister chromatid cohesion. Science *321*, 563–566.

Rowland, B.D., Roig, M.B., Nishino, T., Kurze, A., Uluocak, P., Mishra, A., Beckouët, F., Underwood, P., Metson, J., Imre, R., et al. (2009). Building sister chromatid cohesion: smc3 acetylation counteracts an antiestablishment activity. Mol. Cell *33*, 763–774.

Schalbetter, S.A., Goloborodko, A., Fudenberg, G., Belton, J.-M., Miles, C., Yu, M., Dekker, J., Mirny, L., and Baxter, J. (2017). SMC complexes differentially compact mitotic chromosomes according to genomic context. Nat. Cell Biol. *19*, 1071–1080.

Tercero, J.A., Labib, K., and Diffley, J.F. (2000). DNA synthesis at individual replication forks requires the essential initiation factor Cdc45p. EMBO J. *19*, 2082–2093.

Uhlmann, F., Lottspeich, F., and Nasmyth, K. (1999). Sister-chromatid separation at anaphase onset is promoted by cleavage of the cohesin subunit Scc1. Nature *400*, 37–42.

Uhlmann, F., Wernic, D., Poupart, M.A., Koonin, E.V., and Nasmyth, K. (2000). Cleavage of cohesin by the CD clan protease separin triggers anaphase in yeast. Cell *103*, 375–386.

Unal, E., Heidinger-Pauli, J.M., Kim, W., Guacci, V., Onn, I., Gygi, S.P., and Koshland, D.E. (2008). A molecular determinant for the establishment of sister chromatid cohesion. Science *321*, 566–569.

Vaur, S., Feytout, A., Vazquez, S., and Javerzat, J.-P. (2012). Pds5 promotes cohesin acetylation and stable cohesin-chromosome interaction. EMBO Rep. *13*, 645–652.

Verzijlbergen, K.F., Nerusheva, O.O., Kelly, D., Kerr, A., Clift, D., de Lima Alves, F., Rappsilber, J., and Marston, A.L. (2014). Shugoshin biases chromosomes for biorientation through condensin recruitment to the pericentromere. eLife 3, e01374.

Wutz, G., Várnai, C., Nagasaka, K., Cisneros, D.A., Stocsits, R.R., Tang, W., Schoenfelder, S., Jessberger, G., Muhar, M., Hossain, M.J., et al. (2017). Topologically associating domains and chromatin loops depend on cohesin and are regulated by CTCF, WAPL, and PDS5 proteins. EMBO J. *36*, 3573–3599.

Wutz, G., St. Hilaire, B.T.G., Ladurner, R., Stocsits, R., Nagasaka, K., Pignard, B., Sanborn, A., Tang, W., Varnai, C., Ivanov, M., et al. (2019). ESCO1 and CTCF enable formation of long chromatin loops by protecting cohesinSTAG1 from WAPL. BioRxiv.

Yu, M., and Ren, B. (2017). The Three-Dimensional Organization of Mammalian Genomes. Annu. Rev. Cell Dev. Biol. *33*, 265–289.

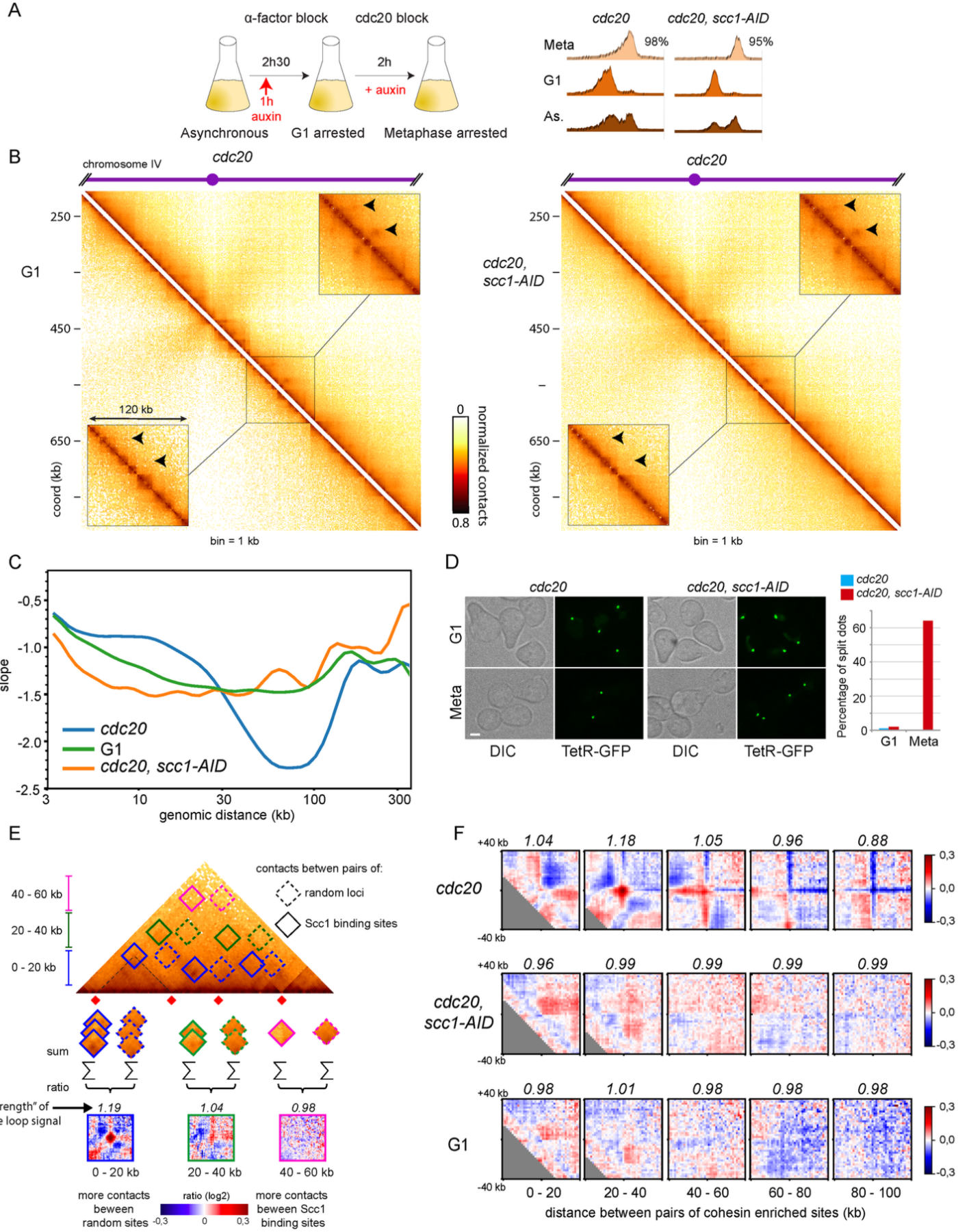
A
α-factor block
cdc20 block
2h30
1h
auxin
2h
+ auxin
Asynchronous
G1 arrested
Metaphase arrested
cdc20
cdc20, scc1-AID
Meta
98%
95%
G1
As.
B
chromosome IV
cdc20
G1
cdc20, scc1-AID
250
450
650
120 kb
coord (kb)
0
normalized contacts
0.8
bin = 1 kb
C
slope
-0,5
-1.0
-1.5
-2.0
-2.5
cdc20
G1
cdc20, scc1-AID
3
10
30
100
300
genomic distance (kb)
D
cdc20
cdc20, scc1-AID
G1
Meta
DIC
TetR-GFP
Percentage of split dots
60
40
20
0
E
contacts betwen pairs of:
random loci
Scc1 binding sites
40 - 60 kb
20 - 40 kb
0 - 20 kb
sum
ratio
"strength" of the loop signal
1.19
1.04
0.98
more contacts beween random sites
ratio (log2)
-0,3
0
0,3
more contacts beween Scc1 binding sites
F
+40 kb
-40 kb
1.04
1.18
1.05
0.96
0.88
0.96
0.99
0.98
1.01
0 - 20
20 - 40
40 - 60
60 - 80
80 - 100
distance between pairs of cohesin enriched sites (kb)

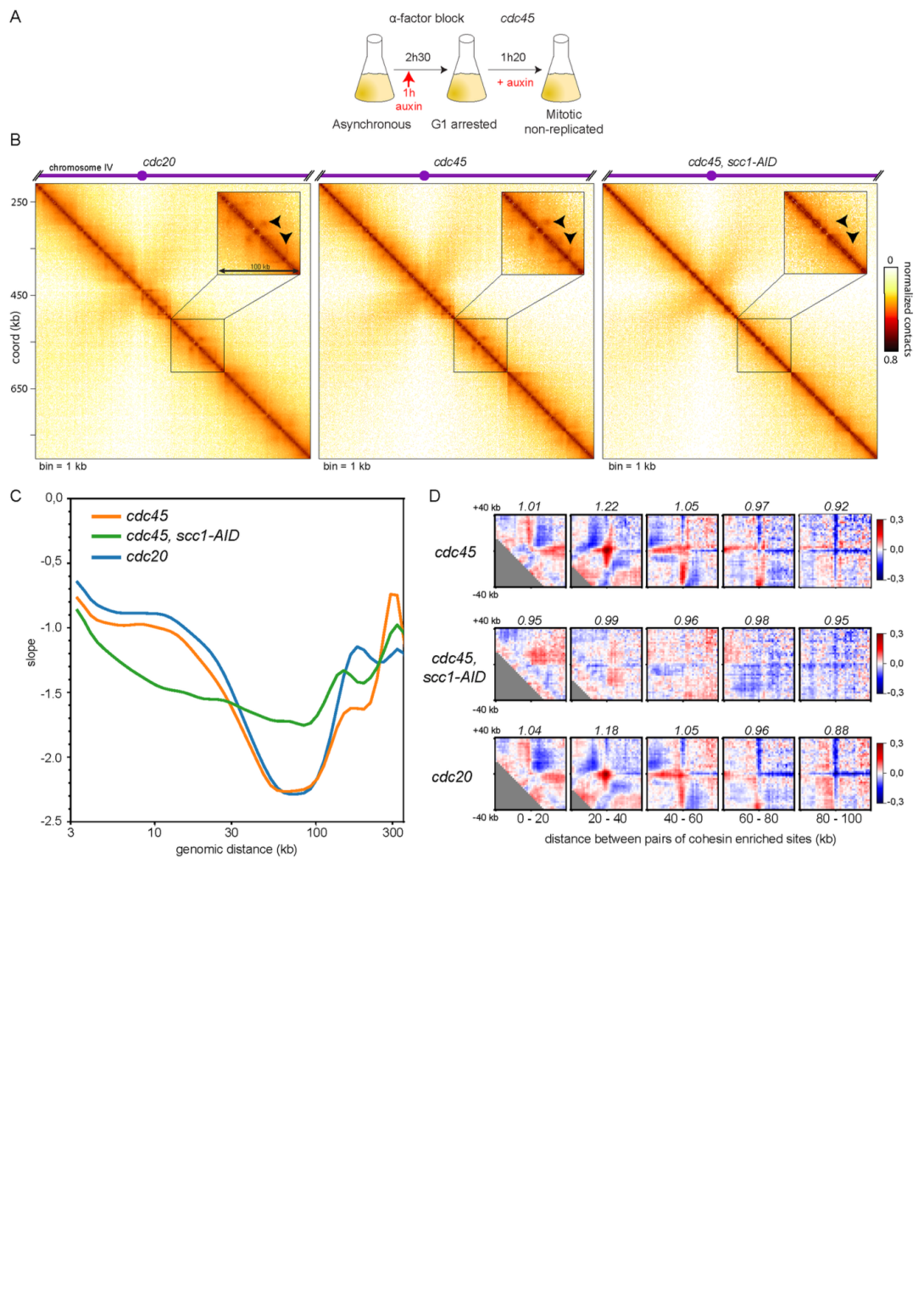
A
α-factor block
cdc45
2h30
1h20
+ auxin
1h
auxin
Asynchronous
G1 arrested
Mitotic
non-replicated
B
chromosome IV
cdc20
cdc45
cdc45, scc1-AID
250
450
650
coord (kb)
100 kb
bin = 1 kb
bin = 1 kb
bin = 1 kb
0
0.8
normalized contacts
C
cdc45
cdc45, scc1-AID
cdc20
0,0
-0,5
-1.0
-1.5
-2.0
-2.5
slope
3
10
30
100
300
genomic distance (kb)
D
+40 kb
-40 kb
cdc45
1.01
1.22
1.05
0.97
0.92
cdc45,
scc1-AID
0.95
0.99
0.96
0.98
0.95
cdc20
1.04
1.18
1.05
0.96
0.88
0,3
0,0
-0,3
0 - 20
20 - 40
40 - 60
60 - 80
80 - 100
distance between pairs of cohesin enriched sites (kb)

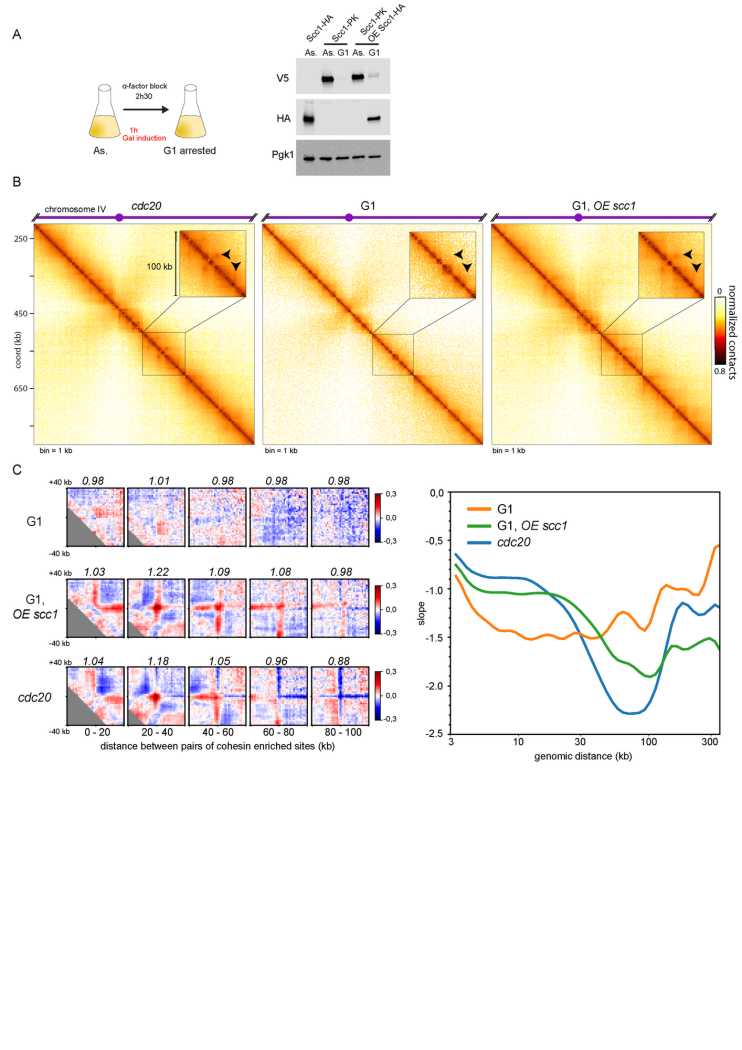
A
Scc1-HA
Scc1-PK
Scc1-PK OE Scc1-HA
As. As. G1 As. G1
V5
HA
Pgk1
α-factor block 2h30
1h Gal induction
As.
G1 arrested
B
chromosome IV
cdc20
G1
G1, OE scc1
100 kb
250
450
650
coord (kb)
bin = 1 kb
bin = 1 kb
bin = 1 kb
0
0.8
normalized contacts
C
+40 kb
-40 kb
G1
G1, OE scc1
cdc20
0.98 1.01 0.98 0.98 0.98
1.03 1.22 1.09 1.08 0.98
1.04 1.18 1.05 0.96 0.88
0,3
0,0
-0,3
0 - 20
20 - 40
40 - 60
60 - 80
80 - 100
distance between pairs of cohesin enriched sites (kb)
G1
G1, OE scc1
cdc20
slope
0,0
-0,5
-1.0
-1.5
-2.0
-2.5
3
10
30
100
300
genomic distance (kb)

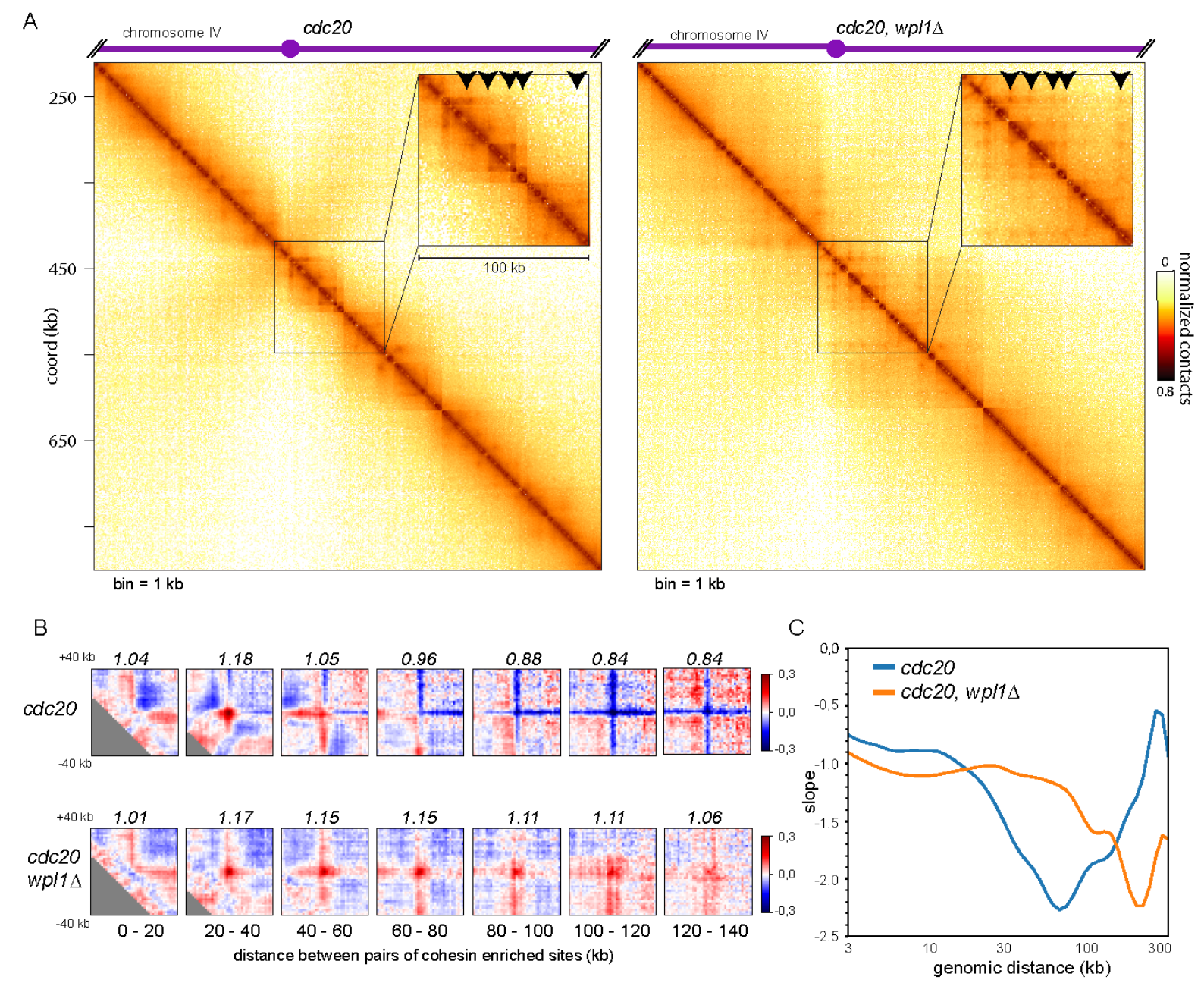
A
chromosome IV
cdc20
chromosome IV
cdc20, wpl1Δ
250
450
650
coord (kb)
100 kb
bin = 1 kb
bin = 1 kb
0
0.8
normalized contacts

B
+40 kb
1.04
1.18
1.05
0.96
0.88
0.84
0.84
cdc20
-40 kb
0,3
0,0
-0,3
+40 kb
1.01
1.17
1.15
1.15
1.11
1.11
1.06
cdc20
wpl1Δ
-40 kb
0 - 20
20 - 40
40 - 60
60 - 80
80 - 100
100 - 120
120 - 140
distance between pairs of cohesin enriched sites (kb)
C
cdc20
cdc20, wpl1Δ
slope
0,0
-0,5
-1.0
-1.5
-2.0
-2.5
3
10
30
100
300
genomic distance (kb)

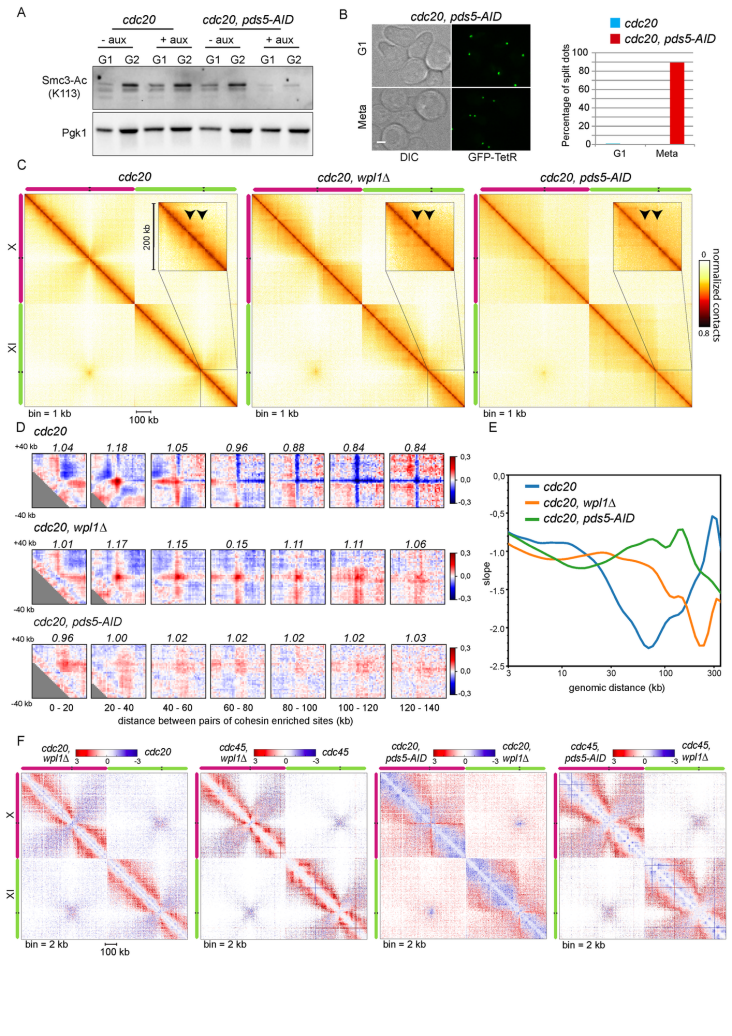
A
cdc20
cdc20, pds5-AID
- aux
+ aux
- aux
+ aux
G1 G2 G1 G2 G1 G2 G1 G2
Smc3-Ac (K113)
Pgk1
B
cdc20, pds5-AID
G1
Meta
DIC
GFP-TetR
cdc20
cdc20, pds5-AID
Percentage of split dots
100
80
60
40
20
0
G1
Meta
C
cdc20
cdc20, wpl1Δ
cdc20, pds5-AID
X
XI
200 kb
normalized contacts
0.8
bin = 1 kb
100 kb
bin = 1 kb
bin = 1 kb
D
cdc20
+40 kb
-40 kb
1.04 1.18 1.05 0.96 0.88 0.84 0.84
0,3
0,0
-0,3
cdc20, wpl1Δ
1.01 1.17 1.15 0.15 1.11 1.11 1.06
cdc20, pds5-AID
0.96 1.00 1.02 1.02 1.02 1.02 1.03
0 - 20
20 - 40
40 - 60
60 - 80
80 - 100
100 - 120
120 - 140
distance between pairs of cohesin enriched sites (kb)
E
cdc20
cdc20, wpl1Δ
cdc20, pds5-AID
slope
0,0
-0,5
-1,0
-1,5
-2,0
-2,5
3
10
30
100
300
genomic distance (kb)
F
cdc20, wpl1Δ
cdc20
cdc45, wpl1Δ
cdc45
cdc20, pds5-AID
cdc20, wpl1Δ
cdc45, pds5-AID
cdc45, wpl1Δ
3
0
-3
X
XI
bin = 2 kb
100 kb
bin = 2 kb
bin = 2 kb
bin = 2 kb

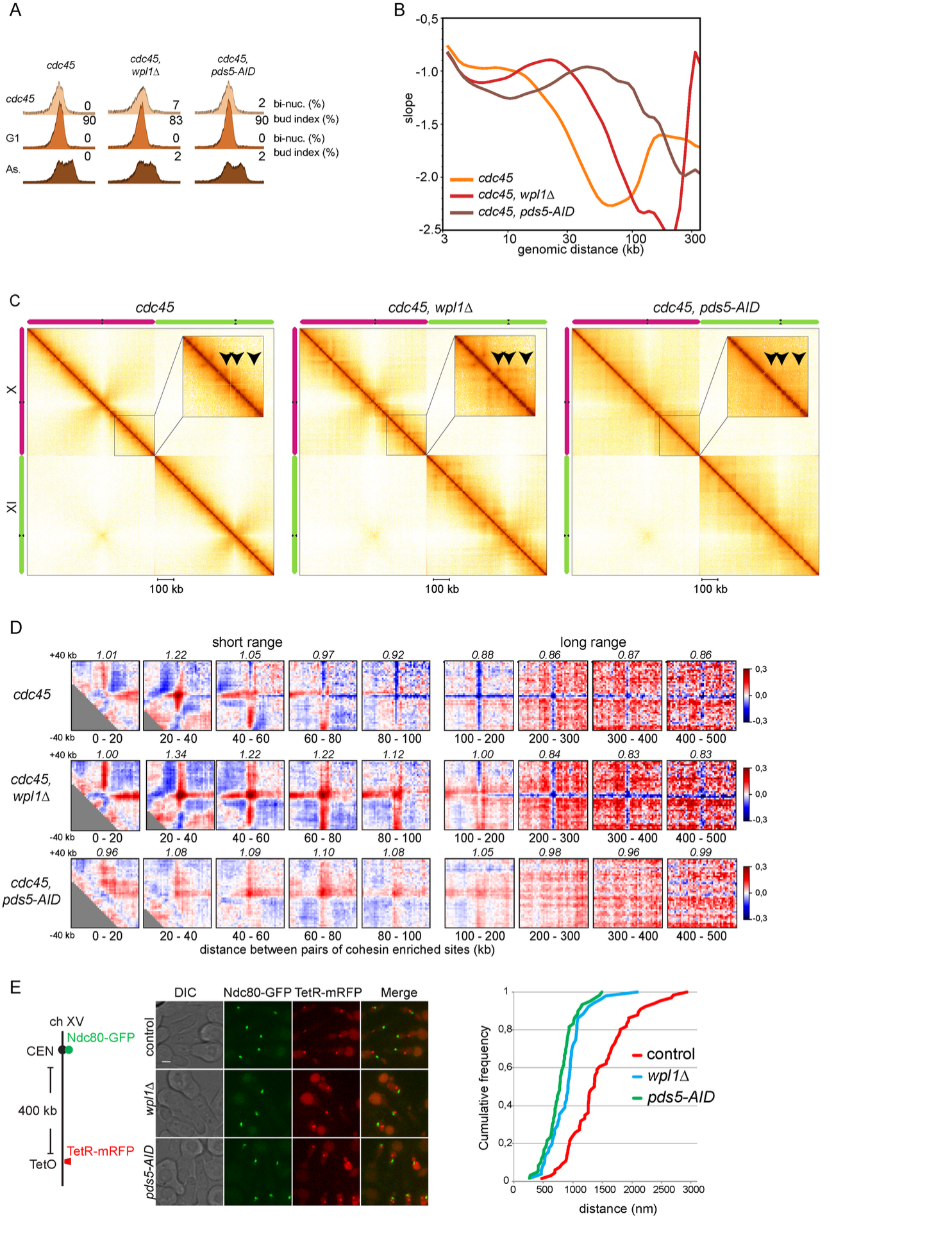
A
cdc45
cdc45, wpl1Δ
cdc45, pds5-AID
cdc45
G1
As.
0
90
0
0
7
83
0
2
2
90
0
2
bi-nuc. (%)
bud index (%)
bi-nuc. (%)
bud index (%)
B
slope
-0,5
-1.0
-1.5
-2.0
-2.5
cdc45
cdc45, wpl1Δ
cdc45, pds5-AID
3
10
30
100
300
genomic distance (kb)
C
cdc45
cdc45, wpl1Δ
cdc45, pds5-AID
X
XI
100 kb
100 kb
100 kb
D
short range
long range
cdc45
cdc45, wpl1Δ
cdc45, pds5-AID
+40 kb
-40 kb
1.01
1.22
1.05
0.97
0.92
0.88
0.86
0.87
0.86
1.00
1.34
1.22
1.22
1.12
1.00
0.84
0.83
0.83
0.96
1.08
1.09
1.10
1.08
1.05
0.98
0.96
0.99
0 - 20
20 - 40
40 - 60
60 - 80
80 - 100
100 - 200
200 - 300
300 - 400
400 - 500
0,3
0,0
-0,3
distance between pairs of cohesin enriched sites (kb)
E
ch XV
CEN
Ndc80-GFP
400 kb
TetO
TetR-mRFP
DIC
Ndc80-GFP
TetR-mRFP
Merge
control
wpl1Δ
pds5-AID
Cumulative frequency
1
0,8
0,6
0,4
0,2
0
0
500
1000
1500
2000
2500
3000
distance (nm)
control
wpl1Δ
pds5-AID

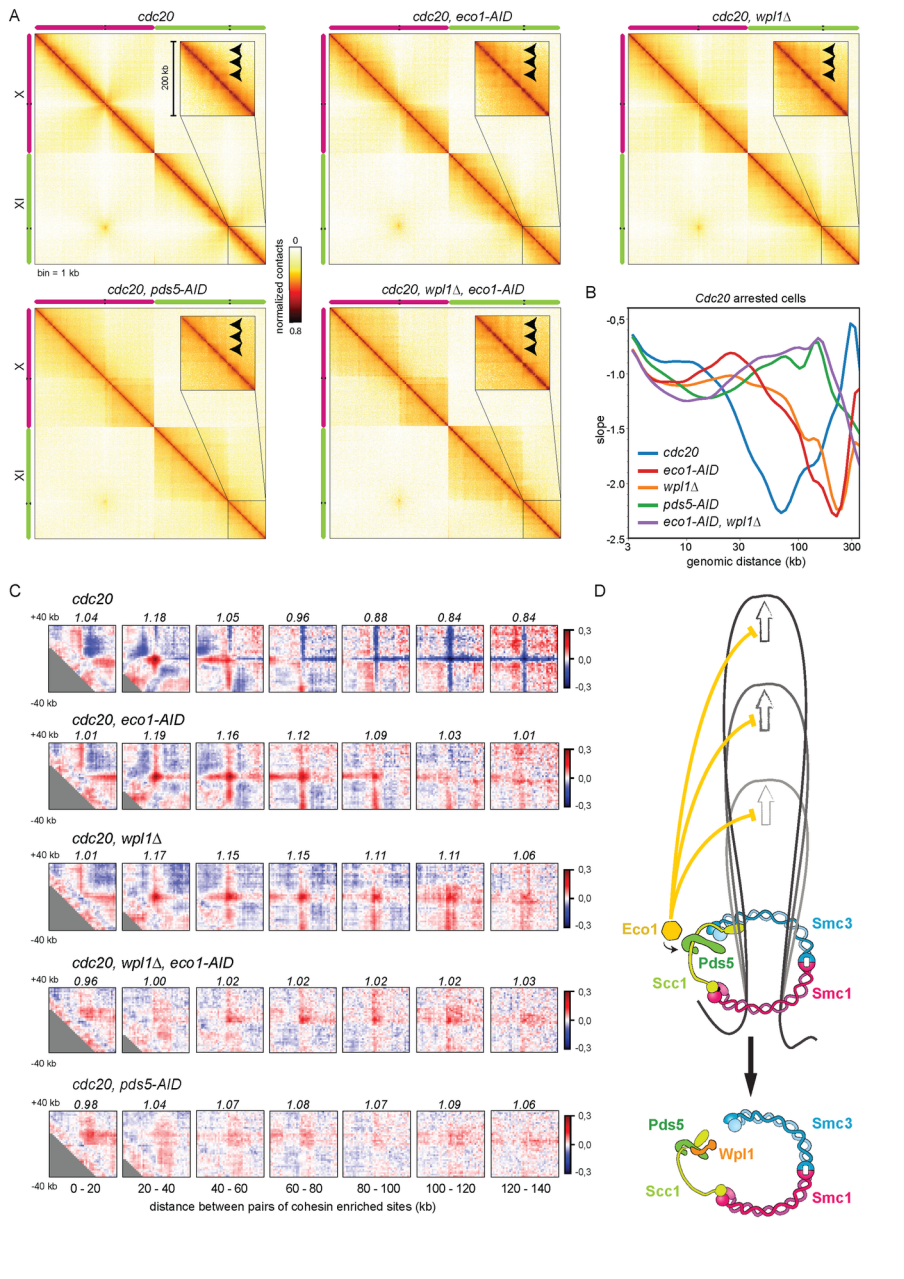
A
cdc20
cdc20, eco1-AID
cdc20, wpl1Δ
cdc20, pds5-AID
cdc20, wpl1Δ, eco1-AID
200 kb
X
XI
bin = 1 kb
normalized contacts
0
0.8
B
Cdc20 arrested cells
slope
-0.5
-1.0
-1.5
-2.0
-2.5
cdc20
eco1-AID
wpl1Δ
pds5-AID
eco1-AID, wpl1Δ
3
10
30
100
300
genomic distance (kb)
C
cdc20
+40 kb
-40 kb
1.04 1.18 1.05 0.96 0.88 0.84 0.84
cdc20, eco1-AID
1.01 1.19 1.16 1.12 1.09 1.03 1.01
cdc20, wpl1Δ
1.01 1.17 1.15 1.15 1.11 1.11 1.06
cdc20, wpl1Δ, eco1-AID
0.96 1.00 1.02 1.02 1.02 1.02 1.03
cdc20, pds5-AID
0.98 1.04 1.07 1.08 1.07 1.09 1.06
0,3
0,0
-0,3
0 - 20
20 - 40
40 - 60
60 - 80
80 - 100
100 - 120
120 - 140
distance between pairs of cohesin enriched sites (kb)
D
Eco1
Pds5
Scc1
Smc3
Smc1
Pds5
Wpl1
Scc1
Smc3
Smc1

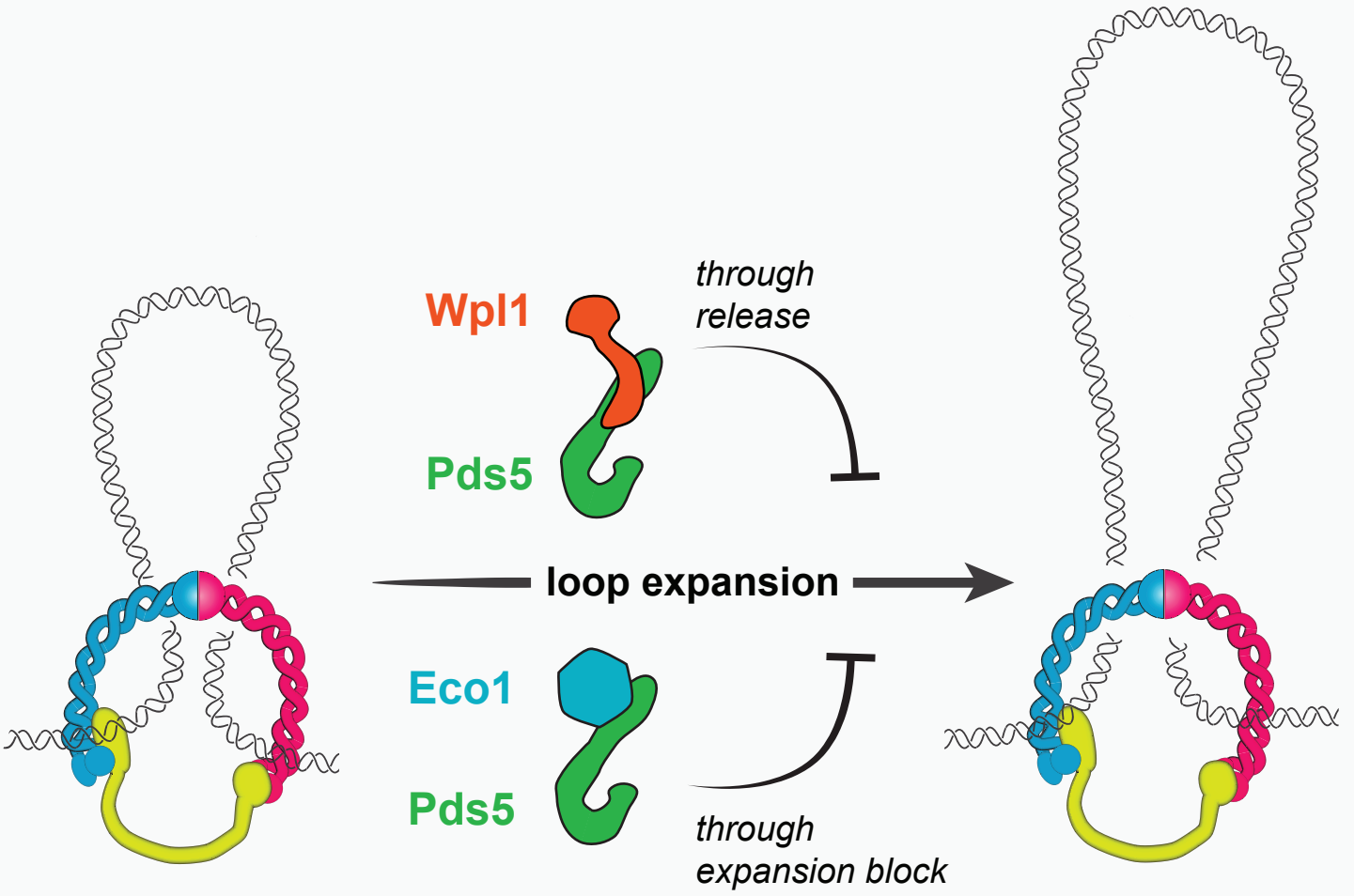
Wpl1
Pds5
through
release
loop expansion
Eco1
Pds5
through
expansion block